High-resolution reconstruction of the beating zebrafish heart

Michaela Mickoleit[1], Benjamin Schmid[1], Michael Weber[1], Florian O Fahrbach[1], Sonja Hombach[1,4], Sven Reischauer[2,3] & Jan Huisken[1]

The heart's continuous motion makes it difficult to capture high-resolution images of this organ *in vivo*. We developed tools based on high-speed selective plane illumination microscopy (SPIM), offering pristine views into the beating zebrafish heart. We captured three-dimensional cardiac dynamics with postacquisition synchronization of multiview movie stacks, obtained static high-resolution reconstructions by briefly stopping the heart with optogenetics and resolved nonperiodic phenomena by high-speed volume scanning with a liquid lens.

Although model organisms such as the zebrafish offer a unique potential for studying cardiac diseases *in vivo*[1], most of the current understanding of early vertebrate cardiac development is based on fixed-tissue data. The shape of a fixed heart is distorted, and it does not resemble any phase of cardiac contraction (**Supplementary Fig. 1** and **Supplementary Video 1**). Alternatively, drugs[2] or morpholinos[3] have been used to stop the heart beat. However, biomechanical forces are essential for proper cardiac morphogenesis and function[4,5]. Hence, cardiac studies should ideally be performed on living tissue in intact organisms, but available microscopes have been too slow to capture the beating heart in three dimensions.

To address this, we built a high-speed SPIM[6,7] setup with double-sided illumination and single-sided detection, dedicated to fast, noninvasive imaging of fluorescently labeled cardiac tissues in zebrafish embryos and larvae. Our system is equipped with a high-numerical-aperture 20× water-dipping detection objective, dual-sided, dual-color light-sheet illumination, an image splitter for simultaneous dual-color acquisition, a fast scientific complementary metal-oxide semiconductor (sCMOS) camera and dedicated solid-state-drive storage (SSD-RAID) (**Supplementary Fig. 2a**). The embedded zebrafish embryo[8] is mounted to motorized stages for accurate and reproducible positioning of the heart in front of the objective lens (**Fig. 1**). We acquired movies of single planes in the beating zebrafish heart with frame rates of ~300–500 frames per second (fps), sampling each cardiac cycle with at least 100 images.

Although high-speed movies in a single plane may be sufficient to describe and quantify a few cardiac properties, for example, valve efficiency[9], they lack the depth information needed to reconstruct the entire beating heart. In SPIM, three-dimensional (3D) information is typically acquired by moving the sample through the light sheet and taking a stack of images, one in each plane. To capture the dynamics of the beating heart, we instead recorded one movie per plane (movie stack), with each movie covering at least one cardiac cycle (**Fig. 1b**). A movie stack across the entire heart consisted of 150–250 movies with a spacing of 1–2 μm between planes. Cardiac contractions in these movies were out of phase and could not be directly assembled into a 3D image. Nevertheless, assuming perfect periodicity of the heartbeat, the same cardiac phase may be found in each plane to reconstruct the heart in 3D.

We designed a postacquisition registration routine to reconstruct the dynamic 3D heart on the basis of similarity. In brief, we calculated the Pearson correlation coefficient between full periods in movies of adjacent planes. We selected and stacked periods with minimal differences to obtain a dynamic 3D image of the beating heart (**Fig. 1c**). Using this routine, we first measured heartbeat variability in zebrafish *Tg(myl7:GFP)* embryos at 48 hours post fertilization (h.p.f.) by determining the period of several consecutive beats in the same heart. We found that consecutive periods indeed varied in their total length by only ~1% on average (**Supplementary Fig. 3a–c**). We observed locally irregular motion of the heart wall only occasionally (**Supplementary Fig. 3d**). In the side view of a four-dimensional (4D)-reconstructed heart, we observed a smooth surface of the cardiac wall (**Fig. 1c** and **Supplementary Videos 2** and **3**), thus indicating that our routine is robust against natural heartbeat variability.

Our synchronization routine is optimized for SPIM data with a high frame rate and a wide dynamic range but may work equally well for slow confocal data for which similar strategies have been developed[10]. However, because of the excessive illumination of the entire heart during a stack in a confocal microscope, only a limited number of planes can be recorded[11]. In contrast, in SPIM we did not observe any such detrimental effects on the sample.

We determined the optimal frame rate and movie duration by comparing their effects on the resulting synchronization quality. We found that synchronization improves with increasing frame rate, with good results achieved with at least 200 fps (**Supplementary Fig. 4a**). We typically used frame rates of 400 fps for short movies, each covering only 2.5 heartbeats (1–1.5 s).

[1]Max Planck Institute of Molecular Cell Biology and Genetics, Dresden, Germany. [2]Max Planck Institute for Heart and Lung Research, Bad Nauheim, Germany. [3]Department of Biochemistry and Biophysics, University of California, San Francisco, San Francisco, California, USA. [4]Present address: Institute of Biochemistry, Genetics and Microbiology, University of Regensburg, Regensburg, Germany. Correspondence should be addressed to J.H. (huisken@mpi-cbg.de).

RECEIVED 3 FEBRUARY; ACCEPTED 16 JUNE; PUBLISHED ONLINE 20 JULY 2014; DOI:10.1038/NMETH.3037

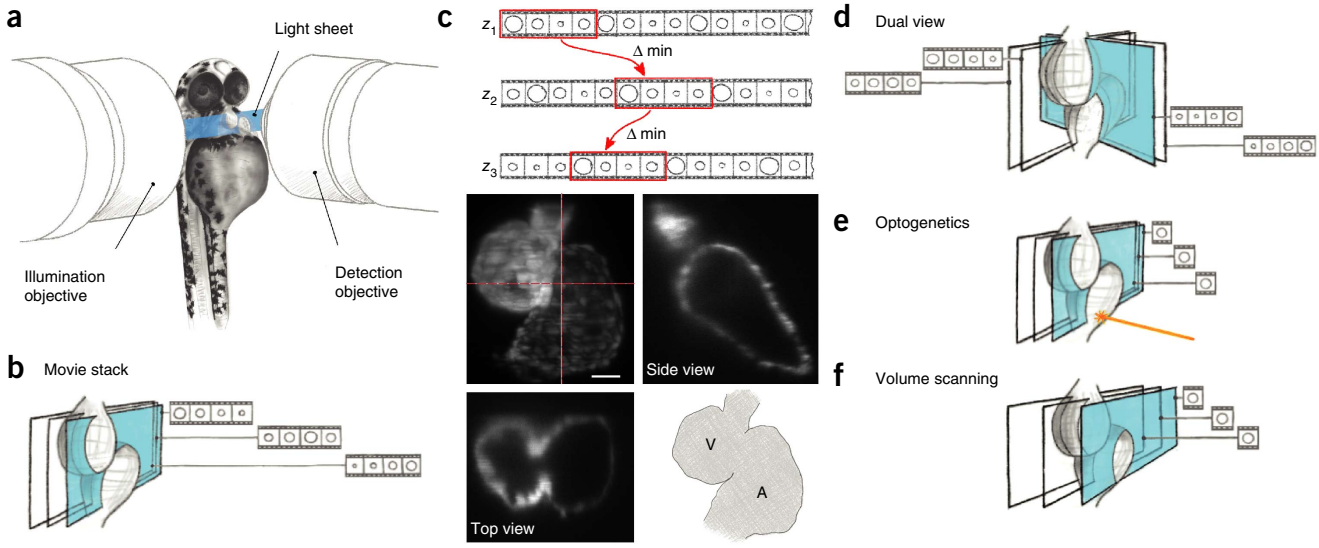

Figure 1 | Cardiac imaging in SPIM. (**a**) Schematic drawing of a zebrafish embryo at the intersection of illumination and detection axes. (**b**) Schematic of movie-stack acquisition (one movie per plane). (**c**) Single-view synchronization via similarity. Top, schematic comparison of three movies. The cardiac cycles with minimal image difference are highlighted. Bottom, reconstructed heart of *Tg(myl7:GFP)* at 48 h.p.f. in front, side and top views, with heart anatomy schematic shown at lower right. A, atrium; V, ventricle. Scale bar, 30 µm. (**d**–**f**) Schematics of dual-view movie stacks with perpendicular recordings (**d**), optogenetic manipulation to stop the heart beat and acquire a *z* stack (**e**) and volume scanning with ETL (**f**).

Lower frame rates, as obtained with conventional charge-coupled device (CCD) cameras (30–100 fps) or confocal line scanning (up to 120 fps)[10], yielded strong deformations in the reconstructed heart (**Supplementary Fig. 4b**). To improve synchronization in low-frame-rate data, the duration of movies had to be increased; for example, at least 4.5 beats per movie were needed at a frame rate of only 67 fps (**Supplementary Fig. 4c**). Alternatively, when only a low-frame-rate camera is available, a static 3D image of the heart can be obtained with prospective gating methods (**Supplementary Fig. 5a**)[12]. Our data demonstrate that the high acquisition speed of SPIM with modern sCMOS cameras (400 fps for 512 × 512 pixels) is key for optimal 3D reconstructions of the beating heart.

Our similarity-based synchronization may eliminate phase delays in the tissue by mistake when the contraction wave propagates along the imaging direction. This is especially problematic during early stages of development, when the heart is a linear tube. To quantify synchronization errors, we prepared a computer-generated heart-tube model that resembled original data in geometry, temporal dynamics and signal-to-noise ratio. Indeed, we obtained incorrect reconstructions when imaging exactly along the contraction axis (**Fig. 2a**,**b**). By measuring the difference between experimental synchronization and theoretical values, we found that an imaging angle of at least 10° is sufficient for proper synchronization of the primitive heart tube (**Supplementary Fig. 6**). Importantly, such synchronization errors might also occur at later developmental stages when the zebrafish heart has looped, and the contraction propagation axis locally falls below 10°, owing to the folded structure of the heart.

To eliminate potential phase-shift errors in experiments, multiple planes could be imaged simultaneously in a SPIM setup with parallel light sheets (**Supplementary Figs. 2b** and **5b**) to provide synchronous movies. Because the simultaneous detection of multiple planes is complicated, we decided to instead make use of the unique ability in SPIM to rotate the sample (**Supplementary Fig. 2b**). After acquisition of one movie stack, we turned the sample by 90° and acquired a second movie stack (**Fig. 1d**). Using the additional information encoded in the second movie stack, we extended our synchronization routine to

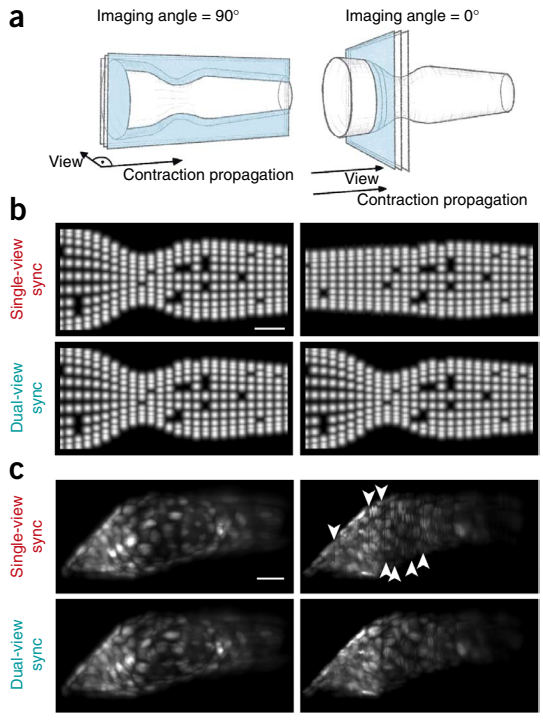

Figure 2 | Dual-view synchronization improves reconstruction at adverse imaging angles. (**a**) Schematic drawing of two synthetic movie stacks of a computer-generated heart-tube model at a favorable imaging angle (left) and at an adverse imaging angle (right). (**b**) Single- and dual-view synchronized (sync) synthetic movie stacks. (**c**) Single- and dual-view synchronization of movie stacks from *Tg(myl7:GFP)* embryos at 30 h.p.f. Arrowheads indicate artifacts. Scale bars throughout figure, 30 µm.

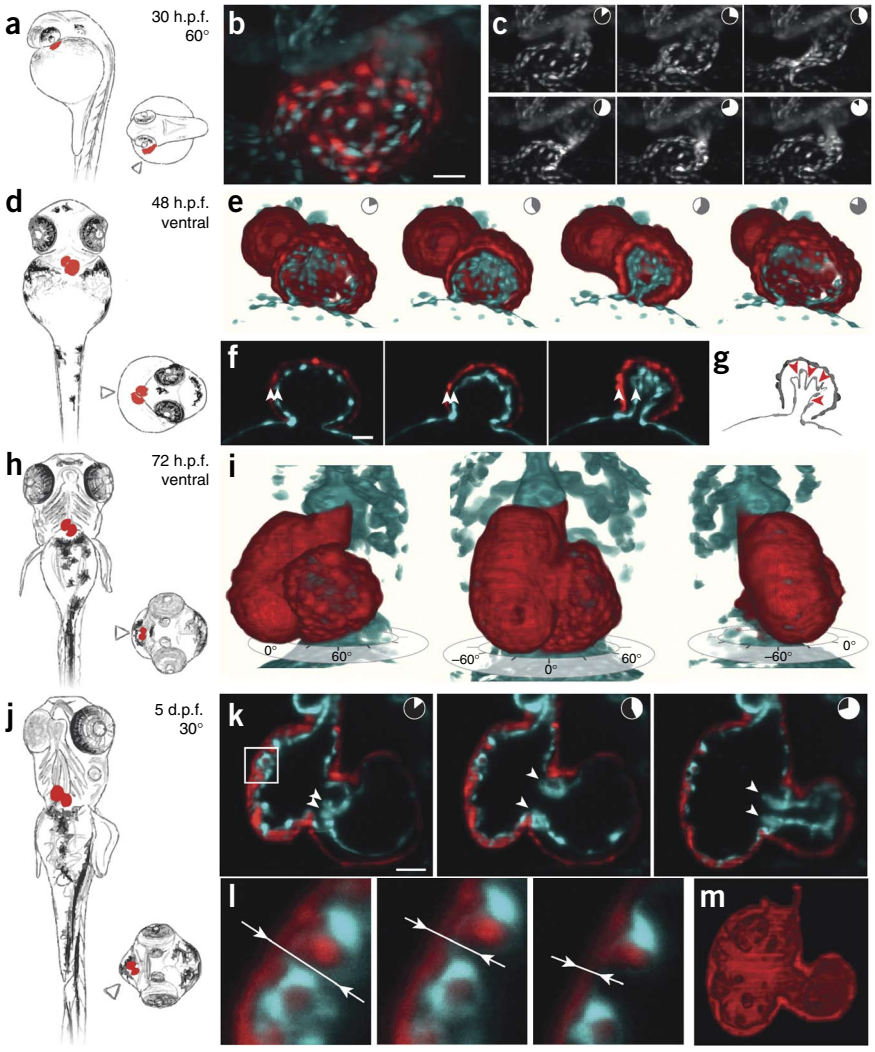

Figure 3 | Reconstructed hearts at different developmental stages. Embryos (*Tg(myl7:DsRed, kdrl:GFP)*) are positioned head up. Red, myocardium; cyan, vasculature. (**a**) Schematic drawing of a 30-h.p.f. embryo at 60°. (**b**) Synchronized movie stack in maximum projection. (**c**) Endocardium at various phases (with time indicated relatively by clock schematic) during the cardiac cycle. (**d**) Schematic drawing of a 48-h.p.f. embryo positioned ventrally. (**e**) 3D rendering of synchronized movie stack cut open in the atrium. (**f**) Stills of the beating heart in one plane of the atrium. Arrowheads mark proximity of myo- and endocardium. (**g**) Schematic drawing of endocardial folds (arrowheads). (**h**) Schematic drawing of a 72-h.p.f. embryo positioned ventrally. (**i**) 3D-rendered heart in three rotated views. (**j**) Schematic drawing of a 5-d.p.f. embryo at 30°. (**k**) Single plane of the heart at different phases in the cardiac cycle. Boxed area is shown enlarged in **l**. Arrowheads indicate the atrioventricular valve. (**l**) Trabeculae with arrows indicating variable thickness of the cardiac wall. (**m**) Bisected heart in a 3D rendering. Scale bars throughout figure, 30 μm.

refine reconstruction, similarly to techniques used in optical coherence tomography[13]. In brief, we aligned both views spatially and temporally on the basis of single-view synchronization results. We iteratively adjusted the phase shifts of each plane in both views alternately while keeping one view fixed to maximize the correlation between both views, until convergence. The synchronization outcome improved in our synthetic data set (**Fig. 2b** and **Supplementary Video 4**) as well as in biological data sets (**Fig. 2c** and **Supplementary Video 5**): both movie stacks were equally well reconstructed and displayed the true shape of the heart. The two movie stacks may even be fused to improve overall resolution, as has been shown for static multiview reconstructions[14,15]. However, additional views require longer acquisition and computation time. We concluded that a single movie stack is sufficient for most of our experiments, whereas the dual-view movie-stack synchronization might be more robust in unsupervised, automatized experiments in which the orientation of the heart is less well defined.

We tested our single-view synchronization routine on data from zebrafish embryos of different developmental stages ranging from 26 h.p.f. to 5 days post fertilization (d.p.f.) (**Fig. 3** and **Supplementary Videos 6–9**) in transgenic lines with labeled myocardial (*Tg(myl7:DsRed)*) or endocardial (*Tg(kdrl:GFP)*) cells. The high-resolution reconstructions are visualized with maximum-intensity projections and 3D renderings to follow characteristic structures of the heart throughout the cardiac cycle. Strikingly, in slow-motion movies, we observed fine details; for example, the distance between endo- and myocardium varied strongly over the course of a heartbeat (**Fig. 3f**,**k**), revealing the incompressibility of the cardiac jelly, which fills the interspace[16]. At the same time, we saw the endocardium folding up upon atrial contraction (**Fig. 3f**,**g**). Probably, as seen in chickens[17], sparse fibrils connect the endo- and the myocardium at certain points, stabilizing the heart and ensuring the opening of the endocardial cavity upon myocardial relaxation. At around 5 d.p.f. the characteristic trabeculae in the ventricle[18] as well as the atrioventricular valve had formed (**Fig. 3k**,**l**), increasing cardiac output and ensuring unidirectional blood flow. We conclude that our synchronization routine is robust for a variety of cardiac shapes of different developmental stages.

Subcellular details and weak expression patterns were still difficult to image in the moving heart, mainly owing to the short exposure time required to suppress motion blur (3 ms). We therefore added an additional light source to our SPIM setup for optogenetic manipulation[19] (**Supplementary Fig. 2b**). We temporally stopped cardiac contractions in *Tg(myl7:Gal4, UAS:NpHR-mCherry, myl7:H2B-GFP)* embryos to acquire high-resolution *z* stacks of the heart (**Fig. 1e**). The shape of the relaxed heart did not correlate to any phase in the cardiac cycle, because both chambers were completely relaxed, but the shape was reproducible in repetitive acquisitions (**Supplementary Fig. 7a**,**b**). During the transient cardiac arrest, we found that the exposure time could be increased for improved image contrast (**Supplementary Fig. 7c**,**d**), and higher magnification provided better spatial resolution (**Fig. 4a**,**b**), such that fine details of filamentous actin (*Tg(myl7:Gal4, UAS:NpHR-mCherry, myl7:lifeactGFP)*)

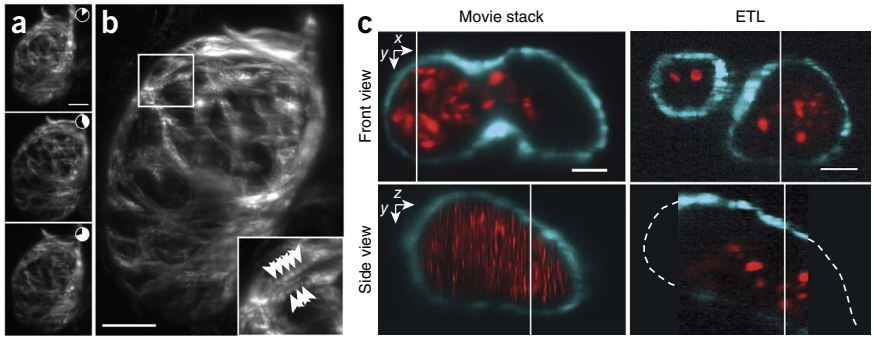

Figure 4 | Optogenetics yields high-resolution images of the heart, and ETL-SPIM captures intracardiac blood flow. (**a**) Three frames from a synchronized movie stack of a 5-d.p.f. embryo (*Tg(myl7:lifeact, myl7:Gal4, UAS:NpHR-mCherry)*). (**b**) Same heart as in **a**, stopped via optogenetics and imaged with higher magnification and longer exposure time. Inset shows enlarged detail of sarcomeres (arrowheads). (**c**) Front and side views of a 48-h.p.f. embryo (*Tg(myl7:GFP, gata1a:DsRed)*) imaged with movie-stack synchronization (left) and ETL-SPIM (right), showing myocardium in cyan and red blood cells in red. Solid vertical lines indicate position of cross section. Scale bars throughout figure, 30 μm.

and individual sarcomeres could be resolved (**Fig. 4b** and **Supplementary Video 10**). The heart can be stopped and imaged repetitively for time-lapse imaging with this approach. The information in static, high-resolution images obtained by optogenetics complements high-speed data from synchronized movie stacks.

Hemodynamics has been intensely studied, yet 3D reconstructions of blood cells circulating through the heart are not available. The distribution of individual blood cells is irregular in subsequent heartbeats, in contrast to the periodically moving myocardial and endocardial cells; our synchronization thus failed to reconstruct the flow of fluorescent blood cells (*Tg(gata1a:DsRed)*) (**Fig. 4c** and **Supplementary Video 11**). To image the blood flow in 3D, we needed to capture the entire heart instantaneously in rapid succession. Volumetric imaging has been achieved by rapidly scanning the light sheet along the detection axis with a galvanometric mirror and, at the same time, refocusing the camera onto the illuminated plane with an electrically tunable lens (ETL) in the detection path[20]. Here, quasisimultaneous dual-color *z* sections with 60 volumes per second were acquired without moving the sample by using an ultrafast camera and a fluorescence splitter (**Supplementary Fig. 2b**). This allowed individual blood cells to be followed as they were pumped through atrium and ventricle (**Fig. 4c** and **Supplementary Video 12**). We used this approach to also image arrhythmic hearts in embryos treated with terfenadine (**Supplementary Video 13**). The ETL-SPIM delivers valuable images of fast irregular movements when postacquisition synchronization algorithms fail.

We have developed a cardiac imaging suite including three variations ranging from static to ultra-high-speed images. 3D reconstructions from high-speed SPIM data offer new insights into the anatomy and function of the intact zebrafish heart without fixation artifacts. The single-view synchronization routine is robust against phase errors and natural heartbeat variability but can easily be supported by dual-view recordings when imaging at adverse angles. Optogenetics and ETL-SPIM further widen the technology's applicability toward higher resolution and higher speed, respectively. We anticipate that our results will serve as the basis for quantitative descriptions of the cellular structure of the beating heart and, complemented by molecular and genetic data, will help understanding of congenital heart diseases.

METHODS

Methods and any associated references are available in the online version of the paper.

Note: Any Supplementary Information and Source Data files are available in the online version of the paper.

ACKNOWLEDGMENTS

This work was supported by the Max Planck Society, the Human Frontier Science Program (CDA 00063/2010-C to J.H.) and a fellowship to M.M. from the Boehringer Ingelheim Fonds. We thank H. Otsuna for assistance with FluoRender and A. Reade, T. Op't Hof, R. Coronel, D.Y.R. Stainier and members of the Huisken laboratory for their comments. Initial work on this project was performed by J.H. in the labs of E.H.K. Stelzer, J. Wittbrodt and D.Y.R. Stainier.

AUTHOR CONTRIBUTIONS

M.M. and M.W. designed and built the SPIM setup. M.M. developed the single-view synchronization routine, performed and analyzed all experiments and visualized the data. B.S. developed the dual-view synchronization algorithm as well as the synthetic-heart-tube model and wrote the software to operate the SPIM setup. M.W. built the hardware for optogenetic manipulation. M.W. and M.M. performed the optogenetic experiments. F.O.F. designed, built, programmed and operated the ETL-SPIM setup. S.H. made the *Tg(myl7:Gal4)* line, and S.R. made the *Tg(myl7:lifeactGFP)* line. J.H. designed and supervised the project. M.M. and J.H. wrote the manuscript with contributions by M.W., B.S. and F.O.F.

COMPETING FINANCIAL INTERESTS

The authors declare no competing financial interests.

1. Bakkers, J. *Cardiovasc. Res.* **91**, 279–288 (2011).
2. Chopra, S.S. *et al. Circ. Res.* **106**, 1342–1350 (2010).
3. Sehnert, A.J. *et al. Nat. Genet.* **31**, 106–110 (2002).
4. Hove, J.R. *et al. Nature* **421**, 172–177 (2003).
5. Auman, H.J., Coleman, H., Riley, H., Olale, F. & Tsai, H. *PLoS Biol.* **5**, e53 (2007).
6. Huisken, J., Swoger, J., Del Bene, F., Wittbrodt, J. & Stelzer, E.H.K. *Science* **305**, 1007–1009 (2004).
7. Huisken, J. & Stainier, D.Y.R. *Opt. Lett.* **32**, 2608–2610 (2007).
8. Kaufmann, A., Mickoleit, M., Weber, M. & Huisken, J. *Development* **139**, 3242–3247 (2012).
9. Scherz, P.J., Huisken, J., Sahai-Hernandez, P. & Stainier, D.Y.R. *Development* **135**, 1179–1187 (2008).
10. Liebling, M., Forouhar, A.S., Gharib, M., Fraser, S.E. & Dickinson, M.E. *J. Biomed. Opt.* **10**, 054001 (2005).
11. Staudt, D.W. *et al. Development* **141**, 585–593 (2014).
12. Taylor, J.M. *et al. J. Biomed. Opt.* **16**, 116021 (2011).
13. Bhat, S., Larina, I., Larin, K., Dickinson, M.E. & Liebling, M. *IEEE Trans. Med. Imaging* **32**, 578–588 (2013).
14. Verveer, P.J. *et al. Nat. Methods* **4**, 311–313 (2007).
15. Preibisch, S., Saalfeld, S., Schindelin, J. & Tomancak, P. *Nat. Methods* **7**, 418–419 (2010).
16. Barry, A. *Anat. Rec.* **102**, 289–298 (1948).
17. Garita, B. *et al. Am. J. Physiol. Heart Circ. Physiol.* **300**, H879–H891 (2011).
18. Liu, J. *et al. Development* **137**, 3867–3875 (2010).
19. Arrenberg, A.B., Stainier, D.Y.R., Baier, H. & Huisken, J. *Science* **330**, 971–974 (2010).
20. Fahrbach, F.O., Voigt, F.F., Schmid, B., Helmchen, F. & Huisken, J. *Opt. Express* **21**, 21010–21026 (2013).

ONLINE METHODS

Fish husbandry and lines. Zebrafish (*Danio rerio*) adults and embryos were kept at 28.5 °C and were handled according to established protocols[21] and in accordance with EU directive 2011/63/EU as well as the German Animal Welfare Act. Transgenic lines *Tg(gata1a:DsRed)*[22], *Tg(kdrl:GFP)*[23], *Tg(myl7:GFP)*[24], *Tg(myl7:DsRed)*[25] and *Tg(UAS:NpHR-mCherry)*[26] were used. Individual positive embryos were chosen randomly from a clutch of 100–300 embryos. The transgenic lines *Tg(myl7:Gal4)* and *Tg(myl7:lifeactGFP)* were generated by Tol2 cloning. No blinding was done.

Fixation and drug treatment. Embryos were fixed in 4% paraformaldehyde (Sigma) for 1 h at room temperature, then incubated in PBT for 30 min. After being rinsed three times with PBS, the embryos were imaged with a stereo microscope (Olympus SZX20) and an sCMOS camera (Hamamatsu, Orca Flash 4.0). To induce arrhythmia, embryos were incubated in 0.1 mM terfenadine (Sigma)[27] for 2–3 h.

Mounting. Embryos were embedded for SPIM imaging in 1.5% low-melting-point agarose (Sigma) in FEP tubes (Bola, S1815-04)[8]. Larvae were embedded in 1.5% low-melting-point agarose inside a glass capillary.

SPIM setup. We custom built a multidirectional selective plane illumination microscopy (mSPIM) setup equipped with double-sided illumination and single-sided detection. The illumination arms are composed of Coherent Sapphire LP lasers (200 mW, 488 and 561 nm), 1-kHz resonant mirrors, cylindrical lenses and Zeiss 10×/0.2 air illumination objectives. The detection arm features a Zeiss W Plan-Apochromat 20×/1.0 detection objective, optional 0.63× and 1.6× magnification, an image splitter (W-View, Hamamatsu) with band-pass 525/50 and long-pass 561 emission filters and a Hamamatsu Flash 4.0 sCMOS camera. The mounted specimen is held in place by a Zeiss Lightsheet Z.1 sample holder and can be oriented and moved with motorized translation and rotation stages (Physik Instrumente). Illumination and detection are controlled by a computer workstation with dedicated SSD RAID 0 storage for fast data streaming.

Single-view synchronization. For single-view synchronization, a movie stack of the heart was acquired consisting of 150–250 movies with a z spacing of 1–2 µm. Usually, the dynamic range in raw images has background values of 50–150 and signal values of 300–1,500, depending on the transgenic line that is imaged. The signal-to-noise ratio (SNR) is typically 50–100 (according to the formula $SNR = \frac{\mu_{sig}}{\sigma_{bg}}$ with μ_{sig} being the average signal and σ_{bg} being the standard deviation of the background).

Synchronization starts at the middle plane and iterates in two independent threads in both directions across the stack. A full period is randomly selected in the middle plane, and the Pearson's correlation coefficient is determined for any possible period in the next plane. The difference is calculated by subtracting the correlation from 1. The period with the minimal difference is then selected for further processing. We use the residual differences to quantify and compare synchronization success. We also tested Euclidean distance and mutual information, alternatively to Pearson's correlation, and found that they performed less accurately and needed more time, respectively. SIFT (scale-invariant feature transform)—a structure- or shape-based comparison method—was disproportionally slow. Therefore we decided to use Pearson's correlation for all our experiments.

Dual-view synchronization. The dual-view synchronization is based on two perpendicular movie stacks (in the following referred to as 'view 1' and 'view 2') and implemented as a Java plugin for Fiji[28]. First, the views were aligned spatially: for both movie stacks, the maximum-intensity projection was computed. View 2 was then rotated by 90° to match the orientation of view 1. The resulting stacks were registered by optimization of the three translational parameters (x, y and z) that aligned view 2 onto view 1 in 3D.

Second, the raw data sets were downsampled for isotropic resolution (with the x spacing of view 1 matching the z spacing of view 2 and vice versa) and cropped, taking into account the registration parameters, such that only the overlapping parts were retained for each view. A specific plane p_1 of view 1 intersects a plane p_2 in view 2 in a vertical line (in the y direction). In total, there are $n_1 \times n_2$ such lines, with n_1 and n_2 being the number of planes in view 1 and view 2, respectively. In both views, this line extends over the number of frames T of one heartbeat, producing two kymographs at each intersection line, for each view. We first shifted the kymograph of p_2 in the time direction (keeping the one for p_1 fixed) and calculated a cost $c_{p1,p2}(\Delta\varphi)$ for each possible relative shift $\Delta\varphi$. These costs were computed via cross-correlation. With an implementation based on the fast Fourier transform, this step usually takes a few minutes for the entire data set. Relative costs were calculated for all intersections between the planes of view 1 and view 2.

In order to find an optimal synchronization, we used an iterative strategy to find the absolute shifts φ_p for each plane that minimized the sum of all relative costs. We initialized all shifts to the result of the single-view synchronization. We then kept the shifts of view 1 fixed and adjusted the shifts of view 2 such that the difference to the previous shifts between neighboring planes was not greater than 1 (i.e., if plane i is shifted by n frames, plane $i + 1$ may be shifted by only $n - 1$, n or $n + 1$ frames). This was performed efficiently (within a few seconds) with dynamic programming. We then kept the shifts of view 2 fixed and adjusted the shifts for view 1. This procedure was repeated until convergence (typically within fewer than ten iterations, so that the overall optimization was performed in less than a minute).

Overall, our strategy shares some principles with existing approaches[13], except for the final computation of absolute shifts. In contrast to previous work, our work exploits the fact that the initial synchronization of the individual views is close to the real solution, and the quality of the synchronization gradually improves as the initial parameters assimilate the true solution. This allows us to exchange the global optimization with the more efficient local search described above.

Optogenetics. For optical manipulation, we coupled a collimated 590-nm LED in the detection arm of our SPIM setup by means of a dichromatic mirror and projected it into the focal plane of the detection objective (**Supplementary Fig. 2b**).

ETL-SPIM. To image the entire zebrafish heart in three dimensions in two colors in a snapshot, we used an electrically tunable lens (ETL, Optotune) in the detection path of the microscope. Tuning its focal length shifts the focal plane of the detection lens remotely so that images of different planes in the sample can be acquired without moving the sample. The light sheet is moved synchronously by a scanning mirror to keep the detected plane illuminated at all times (**Supplementary Fig. 2b**)[20].

To obtain well-defined positions of the image plane, we modulated the focal length of the ETL sinusoidally. The images were therefore not equidistantly spaced across the volume. However, it was straightforward to reconstruct volumes because the position of the image along the detection axis was well defined. The position of image i is $y_i = A\cos(2\pi\, \nu_{ETL}\, i/\nu_{cam} + \varphi)$ where A is the amplitude, ν_{ETL} is the frequency determined by the ETL, ν_{cam} is the frame rate of the camera, and φ is the relative phase between the camera and the ETL. For $\varphi = 0$, identical planes are imaged in the first and the second half of the period $\tau_{ETL} = 1/\nu_{ETL}$, i.e., the 'descending' and the 'ascending' part of the cosine, respectively. We transformed the acquired stack with irregular spacing along y into an equally spaced stack by interpolation. The central planes located around $y_i = 0$ were imaged at equal time intervals of $\tau_{ETL}/2 = 1/2\nu_{ETL}$. However, other planes were imaged with more-asynchronous time intervals, especially the planes $y_i = A$ and $y_i = -A$, which were imaged twice in short succession with time interval $1/\nu_{cam}$ (i.e., by two successive frames), but then only after $1/\nu_{ETL}$ (i.e., an entire ETL period).

For acquisitions with the 20× detection lens, the ETL (EL-10-30-VIS-LD, Optotune) provided an amplitude of $A = 48$ µm when driven at $\nu_{ETL} = 30$ Hz. The CMOS camera (DIMAX 4s, pco) recorded 158 images during each period, thus resulting in 79 different planes being recorded at an average frequency of $2\nu_{ETL} = 60$ Hz. To record two fluorophores in parallel, an image-splitting optic (W-View Gemini, Hamamatsu) was mounted in front of the camera to image green and red fluorescence side by side onto the sensor.

Synthetic heart. We created a 4D phantom heart that resembles original data in terms of heart geometry, temporal dynamics and signal-to-noise ratio. According to real data of a 2-d.p.f. zebrafish embryo, we modeled the heart as a straight conical cylinder, 225 µm in length, with 50-µm and 29-µm radii on the inflow and outflow ends, respectively. Cells were evenly distributed on the surface of the cone via grid points of a 23 × 25 mesh, so that the probability that a given grid point held a cell was 70%. The cells themselves were modeled as Gaussian clouds with an isotropic spatial s.d. of 3.4 µm and a maximum intensity of 1,486.

The heartbeat was modeled as a Gaussian invagination, in which the maximum invagination was 50% of the radius at the corresponding location, and the spatial s.d. was 24 µm. The period of the heartbeat was 0.7 s.

The heart was then sampled at discrete pixel locations to create the artificial image data. Sampling parameters were set according to our microscope parameters: pixel width and height were 0.45 µm, and z spacing was 2 µm. Per heartbeat, 233 frames were created, corresponding to a camera frame rate of 333.2 fps. Random Gaussian noise was added to each pixel value as measured in real data (mean, 106.6; s.d., 4.5). At each image plane, three heartbeats were created, starting at random offsets in the heart cycle. The offsets were kept for later evaluation of the synchronization methods. The heart phantom was sampled from various orientations to simulate different imaging angles and to validate the corresponding quality of synchronization.

Visualization. 3D and 4D data were visualized with Fiji[28] for maximum projections and single slice sections or with FluoRender for volume rendering.

21. Nüsslein-Volhard, C. & Dahm, R. *Zebrafish* (Oxford University Press, 2002).
22. Traver, D. *et al. Nat. Immunol.* **4**, 1238–1246 (2003).
23. Jin, S.-W., Beis, D., Mitchell, T., Chen, J.-N. & Stainier, D.Y.R. *Development* **132**, 5199–5209 (2005).
24. Huang, C.J., Tu, C.T., Hsiao, C.D., Hsieh, F.J. & Tsai, H.-J. *Dev. Dyn.* **228**, 30–40 (2003).
25. Chi, N.C. *et al. Genes Dev.* **22**, 734–739 (2008).
26. Arrenberg, A.B., Del Bene, F. & Baier, H. *Proc. Natl. Acad. Sci. USA* **106**, 17968–17973 (2009).
27. Langheinrich, U., Vacun, G. & Wagner, T. *Toxicol. Appl. Pharmacol.* **193**, 370–382 (2003).
28. Schindelin, J. *et al. Nat. Methods* **9**, 676–682 (2012).

doi:10.1038/nmeth.3037